NASA Contractor Report 181768

Development and Simulation Study of A New Inverse-Pinch High Coulomb Transfer Switch

Sang H. Choi

Information & Control Systems, Incorporated
Hampton, Virginia

Contract NAS1-17685

May 1989

National Aeronautics and
Space Administration

Langley Research Center
Hampton, Virginia 23665

FOREWORD

The work described in this report was performed by Information & Control Systems, Incorporated (ICS) under Contract Number NAS1-17685 for the National Aeronautics and Space Administration, Langley Research Center, Hampton, Virginia. The work was sponsored by the Space Systems Division, High Energy Science Branch at Langley Research Center. Dr. N. W. Jalufka was the NASA Technical Representative monitoring this contract. Dr. S. H. Choi directed the technical effort at ICS.

ABSTRACT

A theoretical study of the inverse-pinch plasma switch was conducted using a computer simulation code. The code was based on a 2-D, 2-temperature magnetohydrodynamic (MHD) model. The application of this code was limited to the disk-type inverse-pinch plasma switch. The results of the computer analysis appear to be in agreement with the experimental results when the same parameters are used.

A novel inverse-pinch plasma switch for closing has been designed and tested for high-power switching requirements. An azimuthally uniform initiation of breakdown is a key factor in achieving an inverse-pinch current path in the switch. Thus, various types of triggers, such as trigger pins, wire-brush, ring trigger, and hypocycloidal-pinch (HCP) devices have been tested for uniform breakdown.

Recently, triggering was achieved by injection of a plasma-ring (plasma puff) that is produced separately with hypocycloidal-pinch electrodes placed under the cathode of the main gap. The current paths at switch closing, initiated by the injection of a plasma-ring from the HCP trigger are azimuthally uniform, and the local current density is significantly reduced, so that damage to the electrodes and the insulator surfaces is minimized. The test results indicate that electron bombardment on the electrodes is four orders of magnitude less than that of a spark-gap switch for the same switching power. Indeed, a few thousand shots with peak current exceeding a mega-ampere and with hold-off voltage up to 20 kV have been conducted without showing measurable damage to the electrodes and insulators.

TABLE OF CONTENTS

LIST OF FIGURES

I. INTRODUCTION

The research efforts in developing the inverse-pinch switch [1] have been directed toward space applications such as high power laser pumping, electric magnetic (EM) launchers and magnetoplasmadynamic (MPD) thrusters. The requirements for such space applications are: long life operation ($> 10^9$ shots or 1 H_z for 30 years), high reliability with no pre-fire (< 1 out of 10^4 failure rate), and high power transfer ($> 10^{10}$ V-A). Achieving the above requirements with conventional or other spark gaps falls short mainly due to the short life span or irregular reproducibility of these devices. In addition, other requirements such as fast rise time, high current handling capability, fast recovery time (which affects the repetition rate), high hold-off voltage, fast thermal energy dissipation, and reduction of component damage have been posed as formidable tasks to be resolved. Thus much effort has been expended in pursuit of a switch which is able to meet the above fundamental requirements.

The inverse-pinch switch is regarded as a promising, long life switch because it disperses the current sheet over a large area, reducing the current density.

Several prototypes [2, 3] of the inverse-pinch switch have been constructed for experimental evaluation. A schematic diagram of one of the prototypes, which is currently in the process of experimental evaluation, is shown in Fig. 1. The basic principle that makes this switch unique is the inverse-pinch of a current sheet which is formed in an annular gap between the inner and outer electrodes which are placed coaxially. Since the field induced in the inverse-pinch geometry interacts with the current, this interaction directs the current sheet to move axially upward, spreading the current sheet over a large active area of the electrodes.

This study encompasses a theoretical analysis by computer simulation of the inverse-pinch plasma switch and the experimental work which was specially performed for exploring

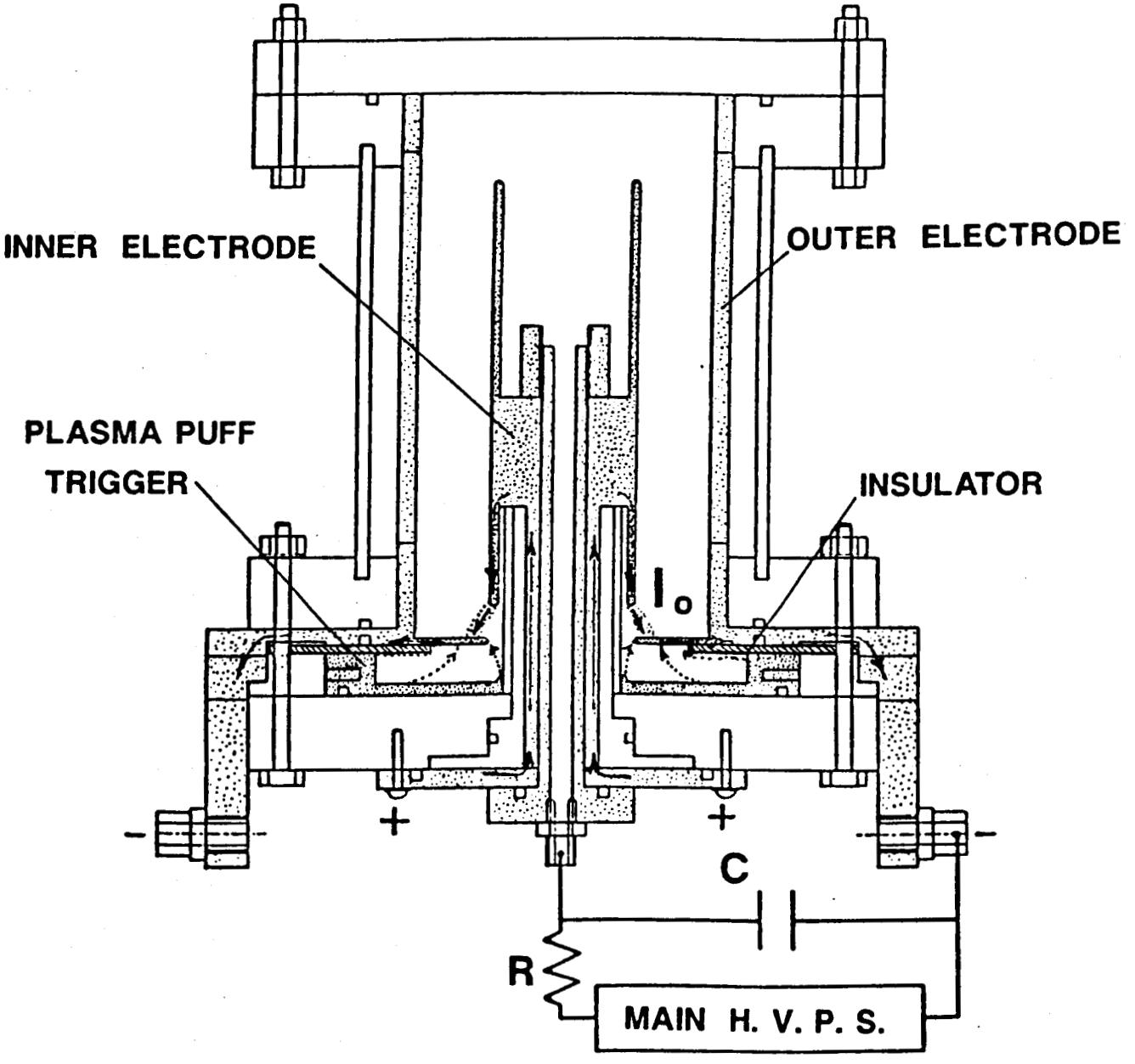

Figure 1. Inverse-pinch switch with plasma puff trigger

a trigger mechanism for uniform breakdown. The computer simulation was developed for the geometry of the disk-type inverse-pinch plasma switch (Fig. 2). In the experiment, four different trigger methods were tested and their results were analyzed on the basis of hold-off voltage and gas pressure.

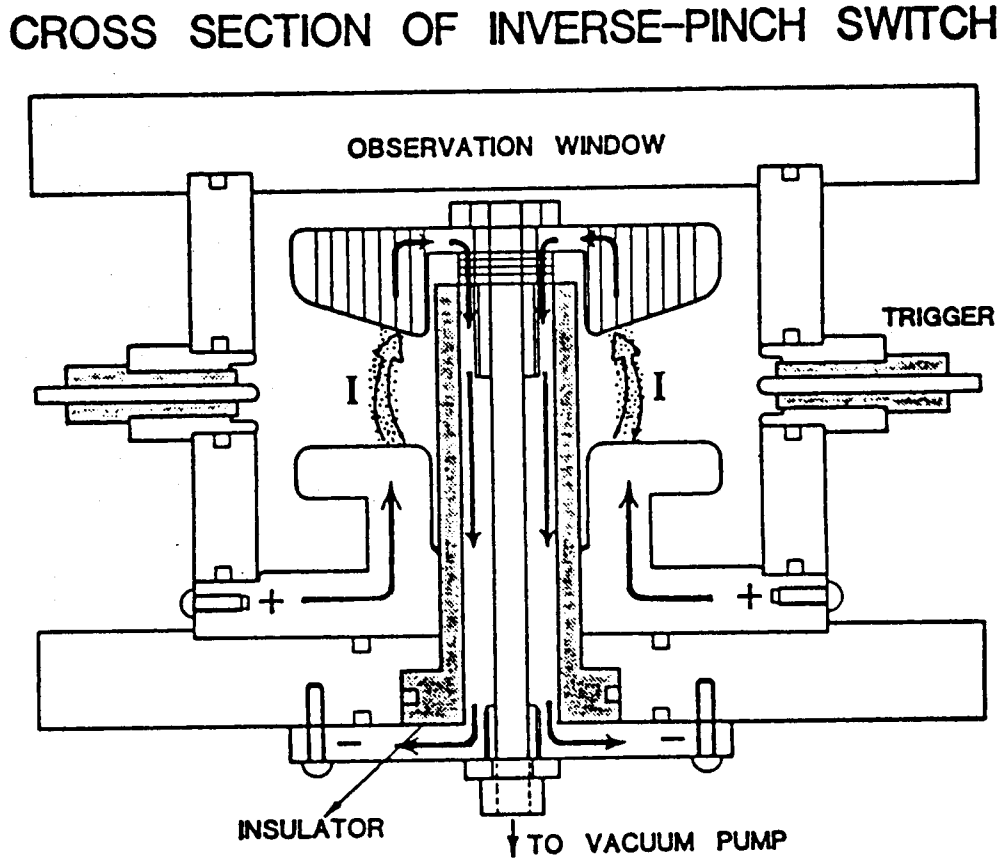

Figure 2. The cross-section view of the inverse-pinch switch which was used for experimental and simulation studies

II. THEORETICAL STUDY

II-1. Introduction.

The theoretical study which includes modeling and numerical simulation is an essential part for the development of the new switch. The important areas of the study are:

1. Analysis of the closing phase with respect to achieving uniform breakdown with less jitter.
2. Analysis of the current sheet behavior in the gap of the annular electrodes during the run-down phase for inductive storage.
3. Understanding and analysis of the plasma dynamic behavior under strong plasma-magnetic field interaction during the opening phase.

The study presented here concentrated on the run-down phase of a switching current based on the inverse-pinch geometry which is shown in Fig. 2.

The major phenomena which appear during switching action are the current sheet formation and its subsequent motion in time and position, the variations of plasma transport parameters and the plasma dynamic behavior. These are the key factors that determine directly or indirectly the rise time of current, the peak current, the wear pattern of electrodes, etc.

The study by numerical simulation determines the plasma parameters at the location and time of the peak current. Subsequently, the plasma parameters could be used for determining the rise time, and the dimension of the switch (including its inductance).

The simulation code for the inverse-pinch geometry was developed for simulating the dynamics of the switch illustrated in Fig. 2. The code could be employed in a parametric study of this switch, and optimal values for various design parameters could be obtained. The results from this study could also be applied to the experimental study for scaling-up

purposes, for an upgrade of the switch hardware, and for the performance analysis of the modified switch.

II-2. MHD and Pulse Forming Network (PFN) Equations.

The frame of simulation code is based on a complete set of equations for plasma fluid model (or MHD) and plasma transport parameters. The set of equations for the plasma fluid model given below were used for the analyses of dynamics of current sheet motion in the disk gap of a co-axial inverse-pinch plasma switch (Fig. 2). The equations were set up for a two-temperature model and the computational code for these equations was developed for the 2-dimensional geometry because of the axial symmetry condition of the switch geometry (Fig. 2).

The continuity equation:

$$\frac{\partial \rho}{\partial t} + \nabla \cdot (\rho V) = 0 \tag{1}$$

The momentum equation:

$$\rho \frac{\partial V}{\partial t} + \rho (V \cdot \nabla) V + \nabla [n(k T_e + k T_i)] = \frac{1}{c}(J \times B) - \nabla \cdot \pi \tag{2}$$

The energy equation for ions:

$$\frac{k}{\gamma - 1} \frac{\partial}{\partial t}(n T_i) + \frac{k}{\gamma - 1} \nabla \cdot (n T_i V) + k n T_i (\nabla \cdot V) + \pi_{\alpha\beta} \frac{\partial}{\partial \chi_\beta} V_\alpha + \nabla \cdot q_i$$
$$= Q_i + \frac{\xi}{2} [J \cdot \nabla T_i + p \nabla \cdot (\frac{J}{\rho})] \tag{3}$$

The energy equation for electrons:

$$\frac{k}{\gamma-1}\frac{\partial}{\partial t}(nT_e)+\frac{k}{\gamma-1}\nabla\cdot(nT_eV)+knT_e(\nabla\cdot V)+\nabla\cdot q_e$$
$$=-Q_i+\eta J^2+W_{ei}(n,T_e) \tag{4}$$

The magnetic field equation:

$$\frac{\partial H}{\partial t}=\nabla\times(V\times H)-\nabla\times(\nu J)-\frac{\xi}{2}\nabla\times\left(\frac{J\times H-1/2\nabla P}{\rho}\right) \tag{5}$$

where

B - the magnetic induction, Gauss.,

c - the speed of light, 2.99793×10^8 m/sec.,

H - the magnetic field strength, Öersted,

J - the current density, amp/cm^2,

k - the Boltzmann's constant, 1.38×10^{-16} ergs/K,

m_e - the mass of electron, 9.1086×10^{-31} kg

m_i - the mass of ion,

n - the number density of electrons or ions, cm^{-3},

P - the pressure, dynes/cm^2,

Q_i - the ion energy change due to electron-ion collisions,

q_e - the conductive heat loss of electrons,

q_i - the conductive heat loss of ions,

T_e - the electron temperature, K,

T_i - the ion temperature, K,

V - the mass velocity vector of the electron and ion fluids,

W_{ei} - the non-relativistic Bremsstrahlung loss rate,

α - the tensor component of coordinate,

β - the tensor component of coordinate,

γ - the ratio of the specific heat,

ρ - the density of the electron and ion fluids,

ξ - the Hall effect exchange coefficient, m_i/e,

η - the resistivity of plasma,

π - the ion viscosity tensor,

ν - the magnetic viscosity.

Equations (1)-(5) are integrated in the switching domain with the electric circuit (or PFN) equations. Since the PFN equations (6)-(9) below were developed based on a standard formation of pulse forming circuit (PFC), as shown in Fig. 3, (6)-(9) could be easily modified according to the formation of the PFN. The terminal voltage drop (V_c) at capacitor of the PFN is

$$V_c = R_E\, I + L_E \frac{dI}{dt} + L_s \frac{dIp}{dt} + L_p \frac{dIp}{dt} + R_p\, I_p \tag{6}$$

And the terminal voltages for the leak and plasma current while switching are the same. Thus

$$R_L\, I_L + L_L \frac{dI_L}{dt} = (L_s + L_p)\frac{dIp}{dt} + R_p\, I_p \tag{7}$$

The total circuit is

$$I = I_L + I_p = \frac{dV\,c}{dt} \tag{8}$$

There is another equation that can be expressed for the z-pinch area. At z-pinch area, the plasma inductance (L_p) varies with respect to time,

$$\frac{dL_p}{dt} = 2 \times 10^9 \left[V_z \ln \frac{R_0}{r} + V_z \frac{r z_t}{R_0^2} + \frac{z \times V_r}{r} \right] \tag{9}$$

where the subscripts o, r, t, and z denote the outside diameter, r-coordinate, bottom tip of anode, and z-coordinate, respectively.

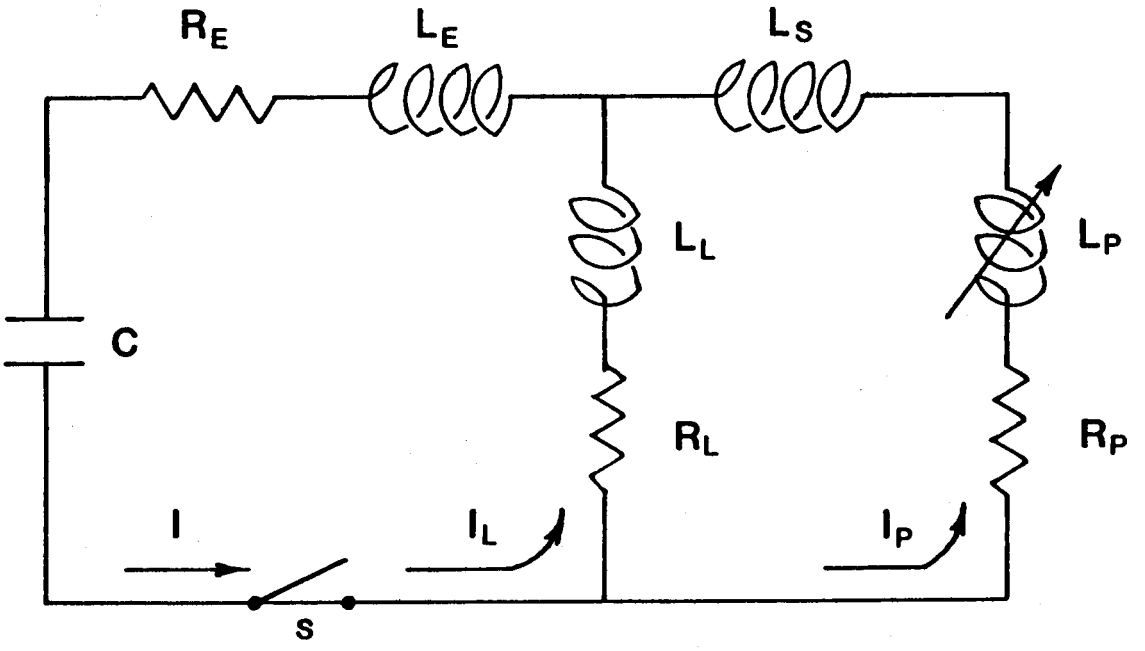

C	External Capacitance
I	Total Circuit Current
I_L	Leak Current
I_P	Plasma Current
L_E	External Inductance
L_L	Leak Inductance
L_P	Plasma Inductance
L_S	Switch Inductance
R_E	External Resistance
R_L	Leak Current Resistance
R_P	Plasma Resistance

Figure 3. The pulse forming network (PFN) diagram

Then the above 9 equations are transformed into numerical forms by employing the alternating direction implicit (ADI) scheme for the time domain of a 2-dimensional geometry. The number of numerical forms after transformation becomes 14 equations. The ADI scheme for the 14 numerical equations forms tri-diagonal matrices and requires the inverse of tri-diagonal matrices for the solution.

The general expressions of the plasma parameters were already included in (1)-(5). These parameters are the ion viscosity tensor (π in (2) and (3)), the conduction loss of ions (q_i in (3)), the conduction loss of electrons (q_e in (4)), the Hall effects (the last terms of (3) and (5)), the ion energy change due to electron-ion collisions (Q_i in (3) and (4)), the Joule heating (η in (4)), the Bremsstrahlung (W_{ei} in (4)), the electron density (n in (2)-(4)), the magnetic viscosity (ν in (5)), and the Coulomb logarithm.

The ion viscosity tensor, π, in a strong magnetic field ($\omega\tau >> 1$) has the following form in the cylindrical coordinate system with z-axis perpendicular to the magnetic field:

$$\pi_{zz} = -0.96\, n_i\, T_i\, \tau_i \Big[\frac{4}{3}\frac{\partial u}{\partial z} - \frac{2}{3}\frac{1}{r}\frac{\partial (rv)}{\partial r}\Big] \tag{10a}$$

$$\pi_{rr} = n_i\, T_i\, \tau_i \Big[0.64\,\frac{\partial u}{\partial z} - 0.32\,\frac{1}{r}\frac{\partial (rv)}{\partial r} - b'(2\omega)\frac{\partial v}{\partial r}\Big] \tag{10b}$$

$$\pi_{\theta\theta} = n_i\, T_i\, \tau_i \Big[0.64\,\frac{\partial u}{\partial z} - 0.32\,\frac{1}{r}\frac{\partial (rv)}{\partial r} + b'(2\omega)\frac{\partial v}{\partial r}\Big] \tag{10c}$$

$$\pi_{r\theta} = \pi_{\theta r} = 2\, n_i\, T_i\, \tau_i \Big[\omega_i\, \tau_i\, b''(2\omega)\frac{\partial v}{\partial r}\Big] \tag{10d}$$

$$\pi_{rz} = \pi_{zr} = 0 \tag{10e}$$

$$\pi_{\theta z} = \pi_{\theta r} = n_i\, T_i\, \tau_i^2\, \omega_i\, b''(\omega)\left(\frac{\partial v}{\partial z} + \frac{\partial u}{\partial r}\right) \tag{10f}$$

where

$$b'(\omega) = \frac{1.2(\omega\tau)^2 + 2.23}{(\omega\tau)^4 + 4.03(\omega\tau)^2 + 2.33} \tag{10g}$$

$$b''(\omega) = \frac{-(\omega\tau)^2 - 2.38}{(\omega\tau)^4 + 4.03(\omega\tau)^2 + 2.33} \tag{10h}$$

The symbols u and v denote the velocity component in the z and r directions.

The time between the ion collisions could be described by

$$\tau_e = \frac{3\sqrt{m_e}\,T_e^{3/2}}{4\sqrt{2\pi}\,\lambda e^4 Z^2 n_i} \tag{11a}$$

$$\tau_i = \frac{3\sqrt{m_i}\,T_i^{3/2}}{4\sqrt{\pi}\,\lambda e^4 n_i Z^4} \tag{11b}$$

$$\omega_i = \frac{e^+ H}{m_i c} \tag{12}$$

where λ is the Coulomb logarithm.

The conduction loss of electrons is described by

$$q_e = -\frac{n_e T_e \tau_e}{m_e}\left[\gamma_{TT}\,\nabla_{\parallel} T_e + \frac{(\beta'_{TT}\omega_e^2\tau_e^2 + \gamma'_{TT})}{(\omega_e\tau_e)^4 + \delta_1(\omega_e\tau_e)^2 + \delta_0}\nabla_{\perp} T_e - \frac{(\beta''_{TT}\omega_e^2\tau_e^2 + \gamma''_{TT})\tau_e}{(\omega_e\tau_e)^4 + \delta_1(\omega_e\tau_e)^2 + \delta_0}(\omega_e \times \nabla T_e)\right] \tag{13}$$

where

$$\gamma_{TT} = f_1(Z) \quad , \quad \gamma'_{TT} = f_2(Z) \quad , \quad \gamma''_{TT} = f_3(Z)$$

$$\beta'_{TT} = f_4(Z) \quad , \quad \beta''_{TT} = f_5(Z) \quad , \quad \delta_0 = f_6(Z) \quad , \quad \text{and} \quad \delta_1 = f_7(Z).$$

The above parameters, as a function of Z, may be found in various publications (i.e., [4]). For $Z = 1$,

$$\gamma_{TT} = 3.1616 \quad , \quad \gamma'_{TT} = 11.92 \quad , \quad \gamma''_{TT} = 21.67$$

$$\beta'_{TT} = 4.664 \quad , \quad \beta''_{TT} = 2.5 \quad , \quad \delta_0 = 3.7703 \quad , \quad \text{and} \quad \delta_1 = 14.79.$$

The conduction loss of ions is

$$q_i = -\frac{n_i T_i \tau_i}{m_i}\left[3.906\nabla_{\|}T_i + \frac{(2\omega_i^2\tau_i^2 + 2.645)\nabla_{\perp}T_i - (2.5\omega_i^2\tau_i^2 + 4.65)\tau_i(\omega_i \times \nabla T_i)}{(\omega_i\tau_i)^4 + 2.70(\omega_i\tau_i)^2 + 0.677}\right] \tag{14}$$

where

$$\omega_i = \left(\frac{e_i}{m_i c}\right) H$$

The last terms of (3) and (5) represent the Hall effects. The exchange coefficient of the Hall effects is m_i/e.

The collision term in (3) and (4) can be described by

$$Q_i = 3k(m_e/m_i)(n_e/\tau_{ei})(T_e - T_i) \tag{15}$$

where τ_{ei} is the electron-ion relaxation time [5]

$$\tau_{ei} = 1.051 \times 10^{16}\, T_e^{3/2}/n_e\,\lambda \quad \mu\text{sec} \tag{16}$$

The resistivity of the plasma used in the numerical calculation is

$$\eta = 3.3 \times 10^{-4}\,\lambda/T_e^{3/2} \quad \text{m}\Omega \cdot \text{cm} \tag{17}$$

The radiation loss due to the non-relativistic Bremsstrahlung may be described by [6]

$$W_{ei}(n,T_e) = \frac{32}{3}\left(\frac{2kT_e}{\pi m_e c^2}\right)^{1/2} \alpha Z^2 r_0^2 n_e n_i c^3 m_e \tag{18}$$

where α is the ionization rate and r_0 is the Larmor radius. For the $e-e$ case, the loss rates are

$$W_{ee}(n,T_e) = 32\left(\frac{2kT_e}{\pi m_e c^2}\right)^{1/2} \alpha r_0^2 n_e^2 c\, k\, T_e \tag{19}$$

The electron density is given by the Saha equation

$$n_e = \left[\frac{(2\pi m_e k T_3)^{3/2}}{h^3}\right]^{1/2} (n_a - n_e)^{1/2} e^{-\frac{qV}{2kT_e}} \tag{20}$$

where n_a is the total concentration of the easily ionized component $(= n_i + n_e)$, V the ionization potential of the ionized components, and h the Planck's constant.

The magnetic viscosity is

$$\nu \cong 6.17 \times 10^{25}\, T_i^{5/2}/n_e\, A^{1/2}\, Z\lambda \tag{21}$$

where T_i is in keV and A is the ratio of m_i and m_p (proton mass). The coulomb logarithm, λ, is here given by

$$\lambda = \ln\left[1 + \frac{3T_e^{3/2}}{2Ze^3\pi^{1/2}n_e^{1/2}}\right] \tag{22}$$

II-3. Applications of MHD Simulation Code.

The simulation code as shown in the block of Fig. 4 and in the flow chart of Fig. 5 was used for the disc-type inverse-pinch plasma switch (Fig. 2) in which the current sheet has a motion in the radial direction. The results are shown in Figs. 6-9. Figure 6 shows the switch current that was fed into the switch from the external high voltage power supply.

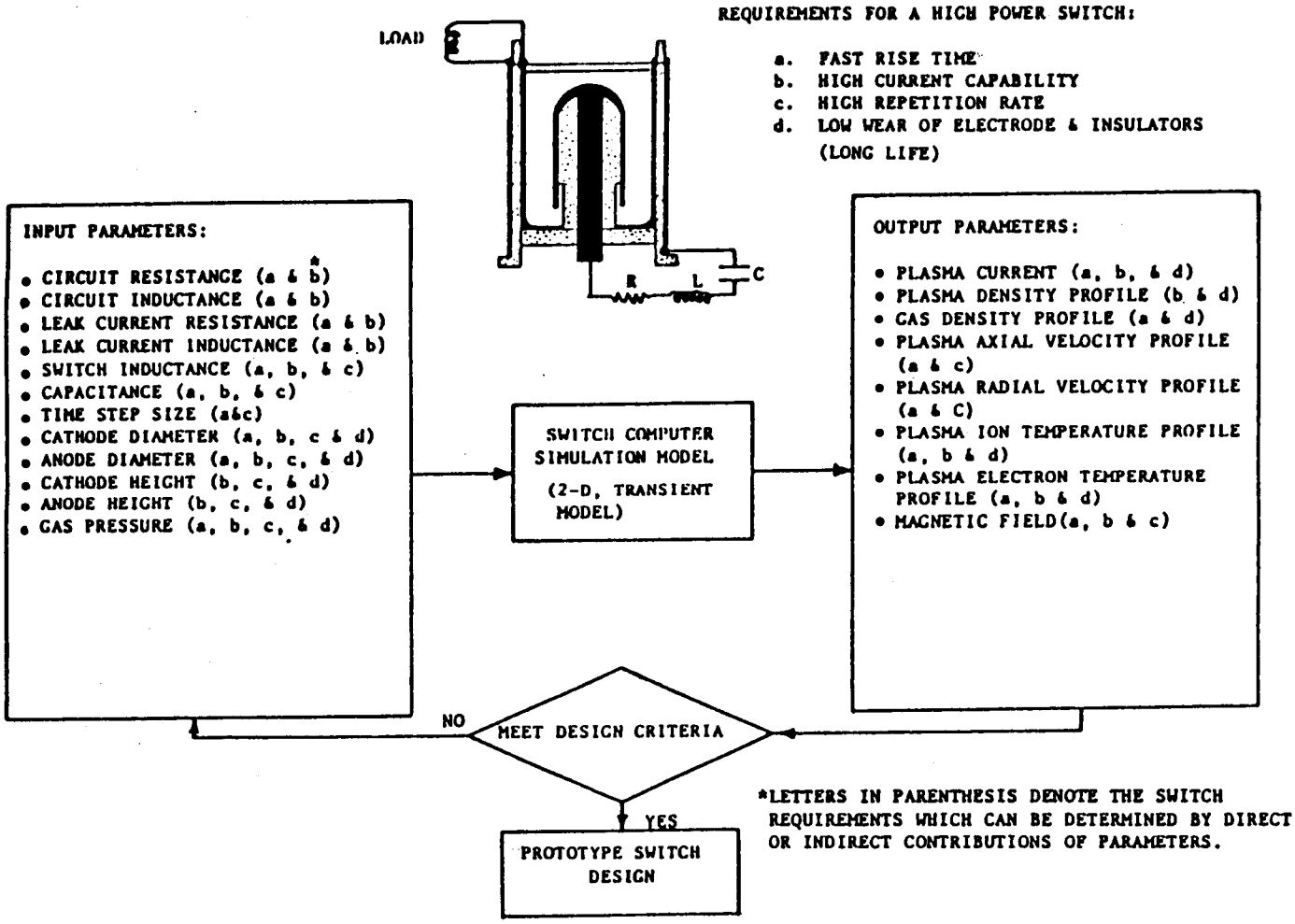

Figure 4. Simulation procedure for a high power inverse-pinch switch

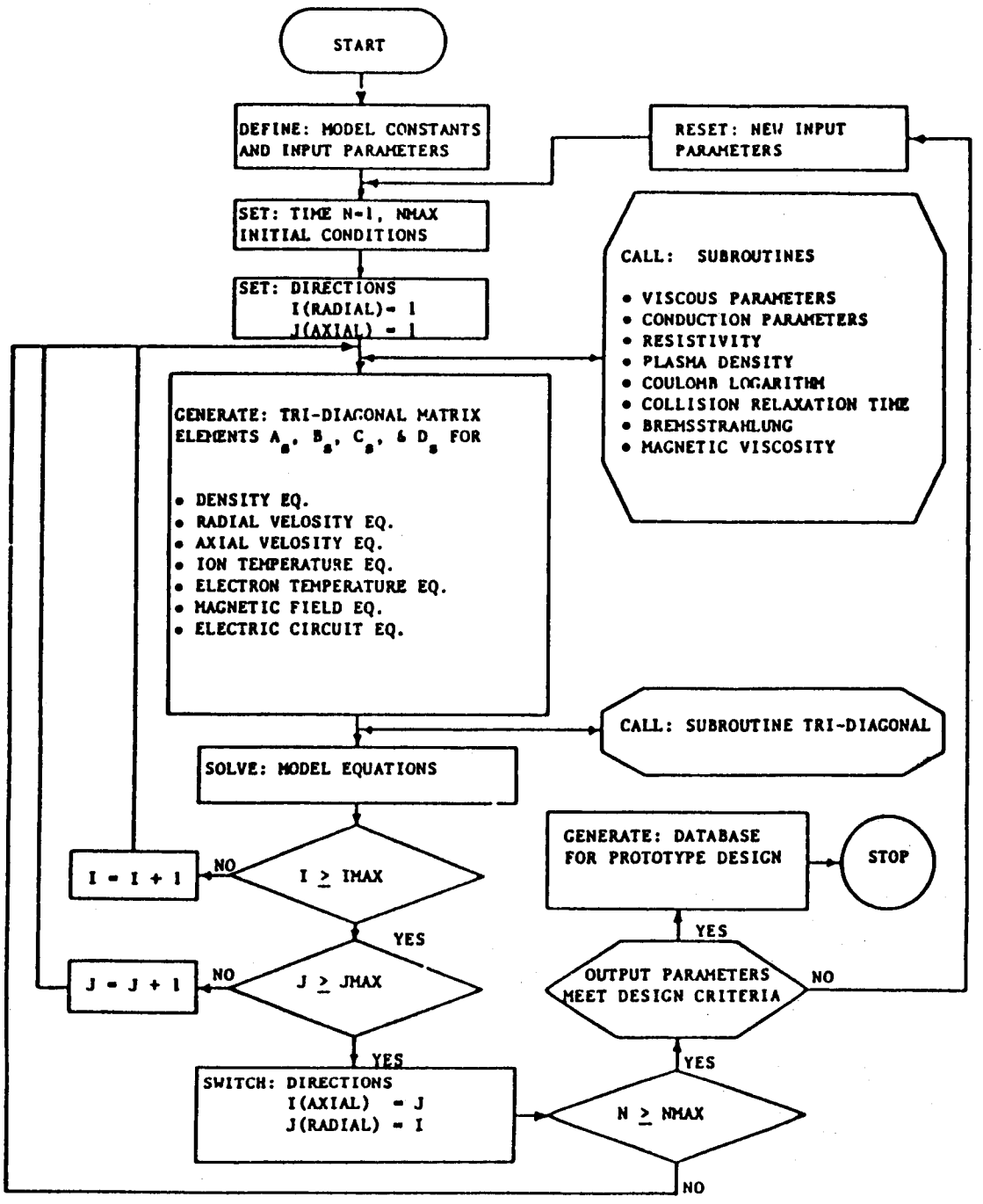

Figure 5. Switch computer simulation model flow chart

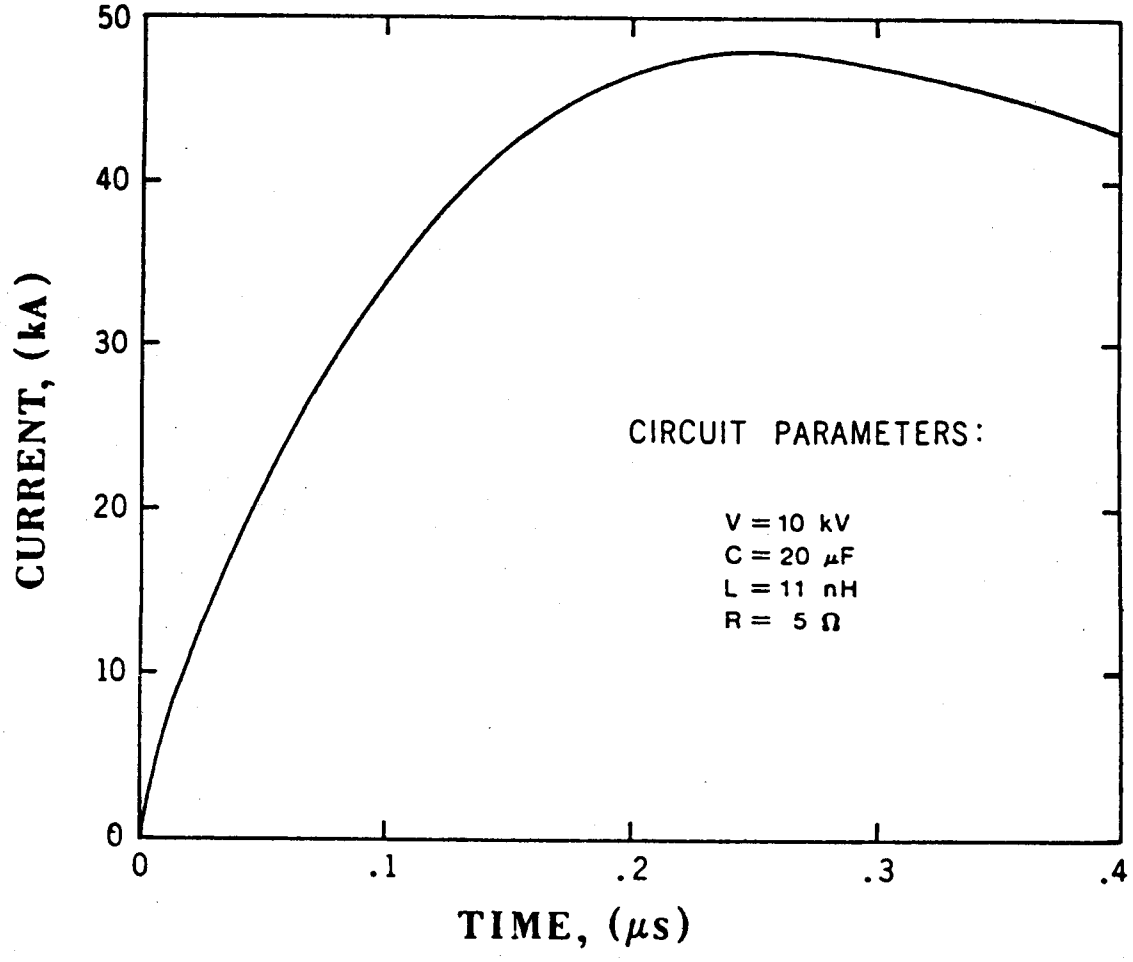

Figure 6. The simulation result of switch current that was fed into the switch (shown in Fig. 5) from the high voltage power supply with respect to time. The circuit parameters were arbitrarily selected for the switch simulation model.

The PFN parameters used in the code are a discharging voltage of 10 kV, a capacitance of 20 μF, a switch inductance of 11 nH, and a resistance of 5 Ω. The peak current in Fig. 6 responds to the rise time of the switch that is, in general, controlled by circuit and switch inductances.

Figures 7 and 8 show the profiles of radial velocity and density along the radial direction at various times before the current reaches the peak level. From Figs. 7 and 8, we can see that the current sheet could move out of the radius of the disc electrodes before the time of the peak current. Such phenomena are also found in the streak mode picture [3]. Figure 9 shows the current sheet velocities as a function of peak current at two different pressures of filled gas (N_2) in both measurement and computer simulation cases. The simulation results are in general agreement with the measured velocities in many cases. The differences may be due to the resolution of streak-photo and accuracy in photo reading, or in some cases to the unpredictable performance of the switch in experiments. Since the reproducibility of the plasma is within the range of an order of magnitude. Accordingly, the results from the simulation study are acceptable and useful for the initial design of the switch.

The MHD and PFN equations which are integrated with the plasma parameters ((10)-(22)) require the initial and boundary conditions according to the physical configuration of the switch which is under consideration. The initial and boundary conditions are determined by the initial PFN parameters and active switching space. In other words, the initial conditions are set by current, voltage, and inductance from the electrical circuit, and the working gas pressure. The boundary conditions are set by the volume of the switch where the plasma current becomes active and described by flow, thermal, and magnetic fields.

With the initial and boundary conditions, the switch domain is divided into a small mesh size to accommodate the steep gradient at the front of the current sheet. Because of non-linear phenomena associated with physical parameters such as Bremsstrahlung,

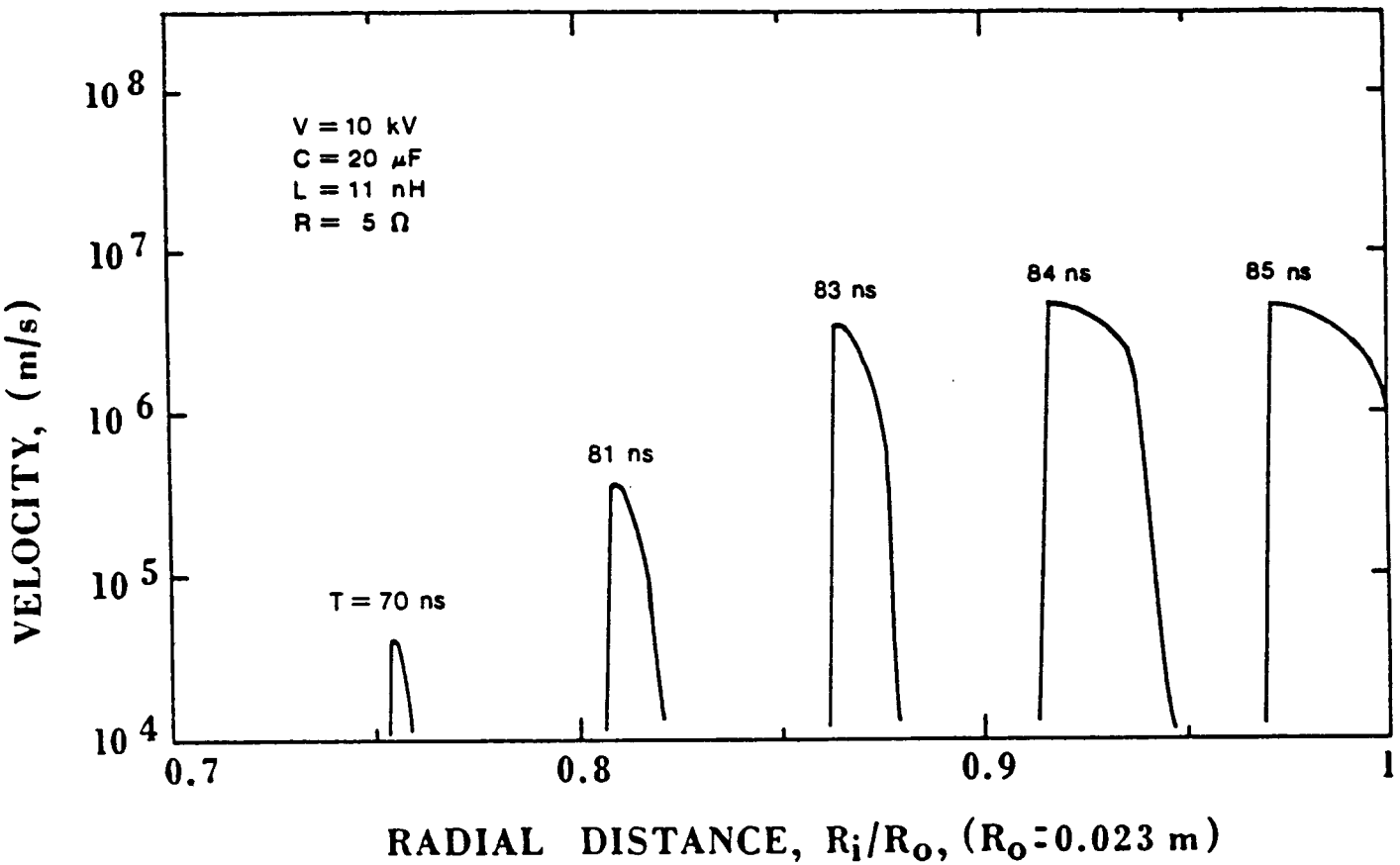

Figure 7. The velocity profiles at various times. The radius ratio $R_i/R_o = 0.7$, signifies the outer radius of the insulator shown in Fig. 5. In this simulation work, the circuit parameters shown at the upper left corner were arbitrarily selected for the performance test of the simulation model.

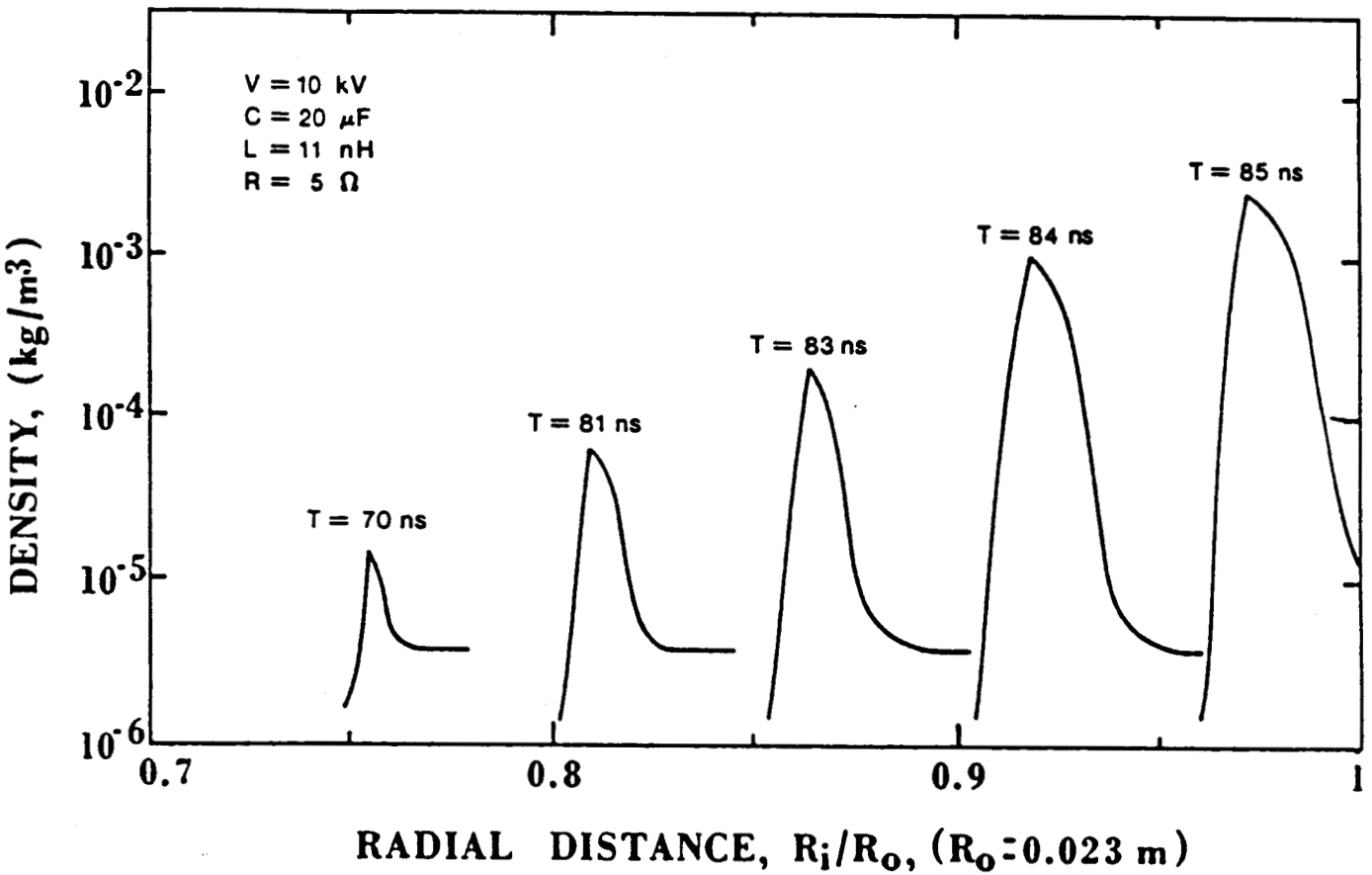

Figure 8. The density profiles at various times before reaching at the peak level of rise time. The radius ratio $R_i/R_o = 0.7$, signifies the outer radius of the insulator shown in Fig. 5. The upper left corner is the circuit parameters which were arbitrarily selected for the performance test of the switch simulation model.

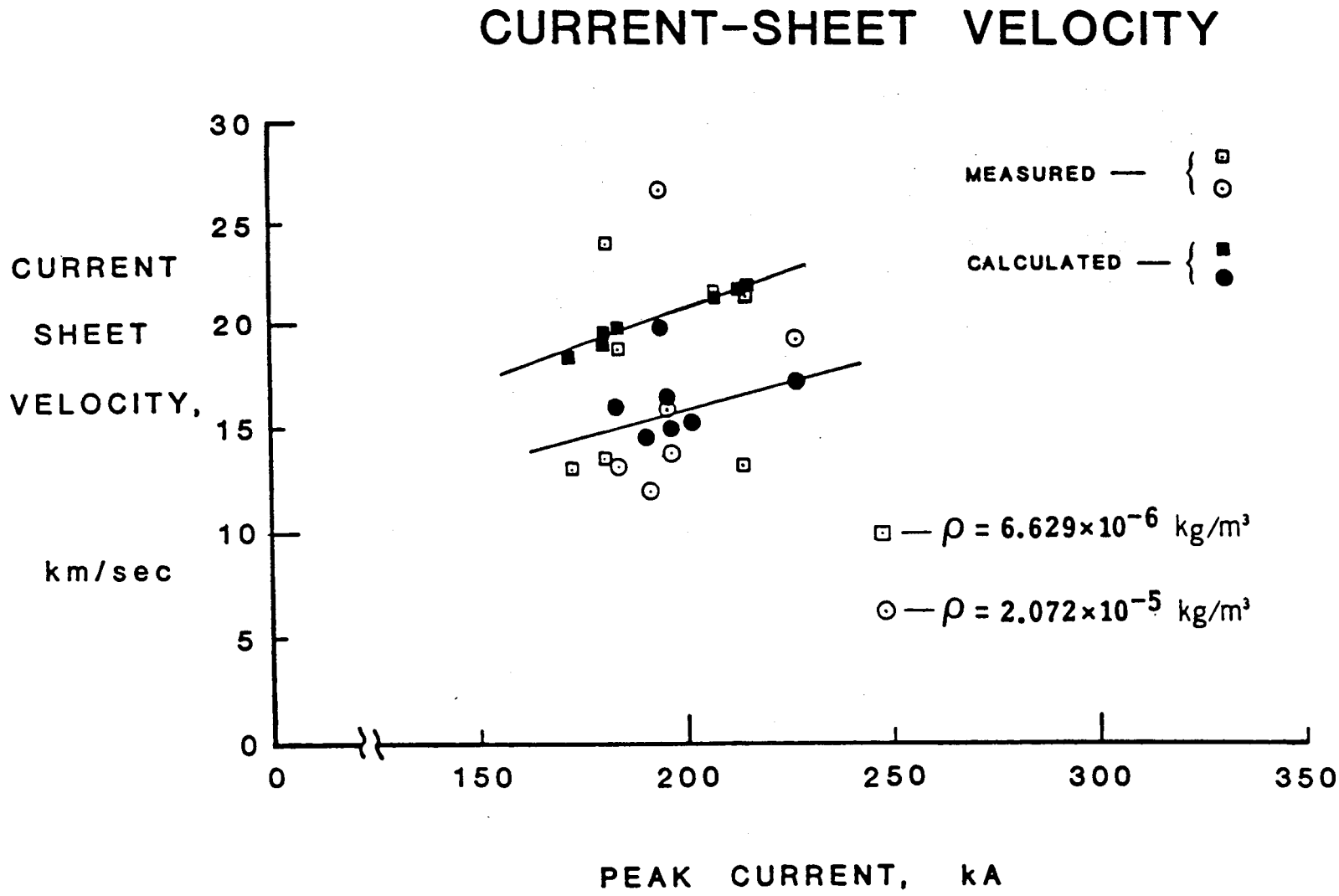

Figure 9. The current sheet velocities at various operations of the switch shown in Fig. 5 were calculated based on the circuit and switch parameters which were obtained from the experiment.

electron-ion collision transfer, viscosity, and conductivity, there is a tendency for the most important physical processes to occur in very thin compressed regions. The simulation code was not written for a thin layer analysis, but it is strongly recommended that the finite difference grid system must resolve very thin layers, and since their locations are not known a priori, an adaptive type of grid should be employed.

III. EXPERIMENTAL WORK

III-1. Introduction.

The inverse-pinch plasma switches (Figs. 1 and 2) require a uniform breakdown around the annular gap for current sheet formation. This uniform breakdown by a trigger is a key factor for successful operation of the inverse-pinch switch.

Several approaches to achieve a uniform breakdown have been attempted. These include trigger pins, ring trigger, wire-brush trigger, and hypocycloidal-pinch (HCP) plasma puff trigger.

The experimental apparatus consists of the capacitor bank, a power supply, a Marx generator for a high voltage trigger pulse, and a vacuum pump unit. The capacitor bank is composed of 18 capacitors in parallel having a total storage energy of 76 kJ, a total capacitance of 61 μF, and a design voltage of up to 50 kV. The trigger pulse, with a 30 ns rise time, is generated by using a Marx generator which amplifies the voltage by a factor of 6. Figure 10 shows a schematic of the inverse-pinch plasma switch experiment. As diagnostic tools, two dual beam oscilloscopes and two image converter cameras (ICC) were employed. One ICC was set with exposure times of 200 ns for the frame mode, while the second ICC was set with exposure times of 200 ns with resolution of 5 ns.

The electrical parameters of the circuit are obtained from Rogowskii coils and voltage dividers. When a Rogowskii coil is coupled with an RC integrating circuit, its output voltage is linearly related to the switching current. By using the capacitor charging voltage and the peak current measured from the Rogowskii coil signal, the switch performance may be rated with a single parameter $P = V \times I$. The Rogowskii coil is accurate to $\pm$ 30 percent when the discharge frequency is greater than 95 kH_z. A vacuum pump is used to evacuate the switch chamber pressure down to 10 mTorr.

Measurements were made to test the characteristics of the wire-brush trigger, HCP plasma puff trigger, and ring trigger mechanisms, as well as the performance of the inverse-pinch switch. These measurements were made with frame photographs, streak photographs, and voltage and current signals on the low pressure side of the Paschen curve. For the inverse-pinch switch (Fig. 1), an initial uniform breakdown is a key factor for obtaining reproducible switching and long life operation. Accordingly, the development of an inverse-pinch switch depends on finding a suitable trigger mechanism. Trigger mechanisms such as the trigger pins [2], ring trigger, wire-brush trigger, and hypocycloidal-pinch (HCP) plasma puff [3] have been tested.

III-2. Trigger Pins.

By using trigger pins with a trigger pulse having 100 ns rise time, the desired uniform breakdown and reproducibility of the inverse-pinch switch were limited [2] to less than 20% at a pressure of 10 mTorr. A fast, high voltage trigger pulse to the trigger pins improved the reproducibility somewhat, but the wear of the trigger pins was significant and the switch therefore had a short life.

III-3. Ring Trigger.

Most recently, the inverse-pinch plasma switch has employed the electron avalanche trigger [7] (or the ring trigger) for uniform breakdown. The sharp edge of the ring trigger was placed at the bottom of the switch facing the inner electrode of the inverse-pinch switch through the annular window between the inner and outer electrodes (Fig. 1 of [7]). Accordingly, when a fast, high voltage trigger pulse of approximately 60 kV from the mini-Marx generator was applied to the gap between the sharp edge of ring trigger and the main inner electrode, which held off 14 kV, the total voltage difference was 74 kV. In low pressure operation ($\leq$ 30 mTorr) of the switch, with the voltage difference of 75

kV, a uniform breakdown by electron avalanche was observed. The frame photographs of the image converter camera show this resulting uniform breakdown (Fig. 2 of [7]). The uniform breakdown with the ring trigger was repeatedly observed only for low pressures. Figure 10 shows the experimental data. The main current signal was measured by the Rogowskii coil while the system parameters which are shown in Fig. 11 were maintained.

III-4. Wire-Brush Trigger.

The sharp edge ring from the ring trigger was removed, and tungsten wires, which had a diameter of approximately 1 mm were embedded with a protrusion of 2 mm in the area where the sharp edge ring was originally. Tests were conducted to find the appropriate pressure range for uniform breakdown. A fast, high voltage trigger pulse of 60 kV and 30 ns rise time was fed into the area between the wire-brush triggers and the main inner electrode of the inverse-pinch switch. The breakdown appears to be irregular and non-uniform at low pressure. However, at the high pressure portion of the Paschen curve, the breakdown became uniform. Typical measurement data are shown in Fig. 12.

III-5. Hypocycloidal-Pinch (HCP) Plasma Puff (HCP^3) Trigger.

The HCP device was invented by J. H. Lee [8] to create a high density and high temperature plasma for nuclear fusion. This device has also been used as a light source for high energy laser (HEL) pumping [9].

Since the invention of the inverse-pinch switch [10], the trigger mechanism has become a key component in achieving a uniform breakdown. Despite the many advantages of the inverse-pinch switch over conventional switches in high power applications, the development of this switch has been slowed by the lack of a suitable trigger mechanism. The HCP device appears to be very suitable for a trigger because it creates a uniform azimuthal plasma which is then compressed. This HCP device has been demonstrated as

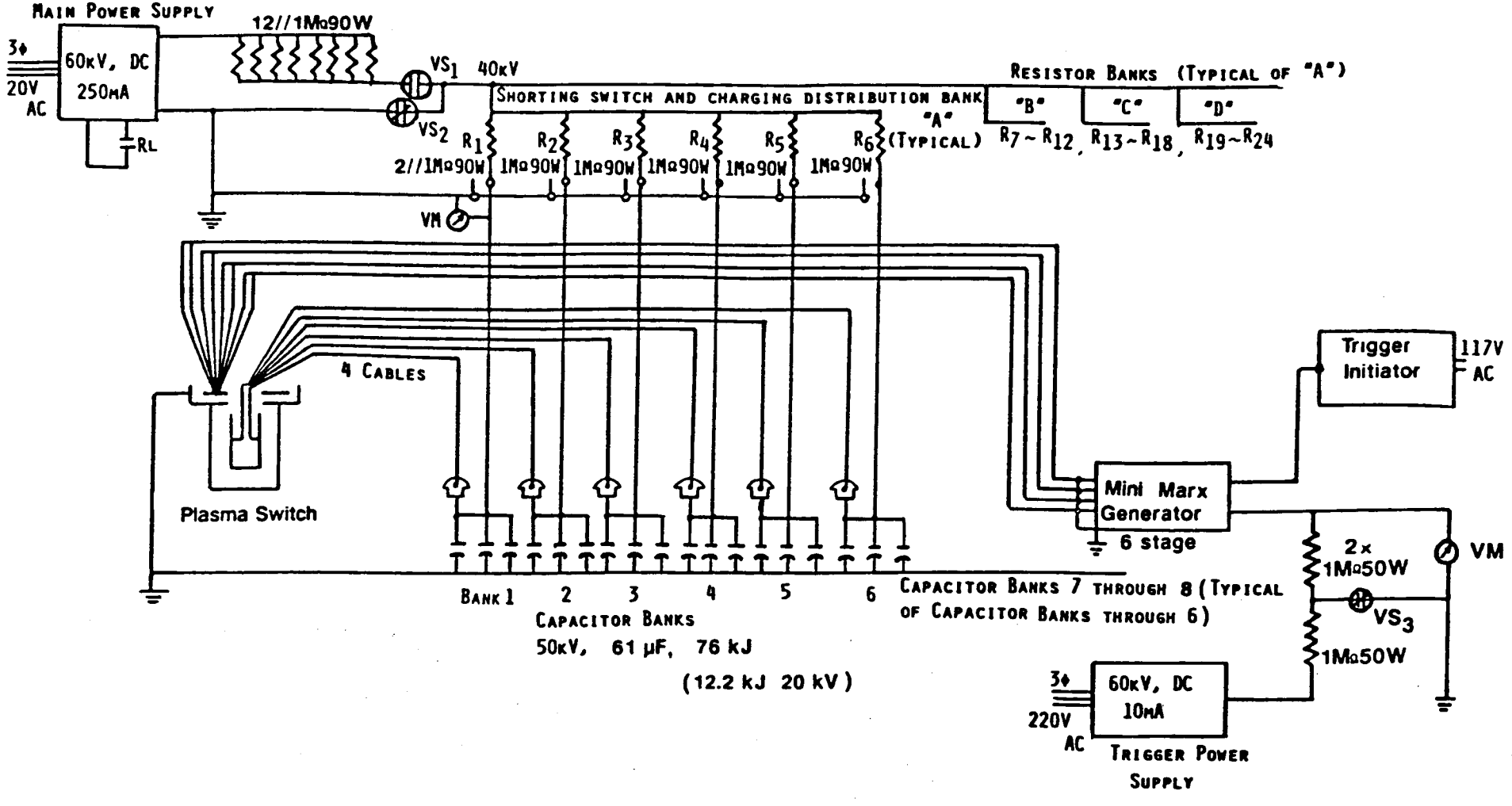

Figure 10. Schematic of inverse-pinch plasma switch experiment

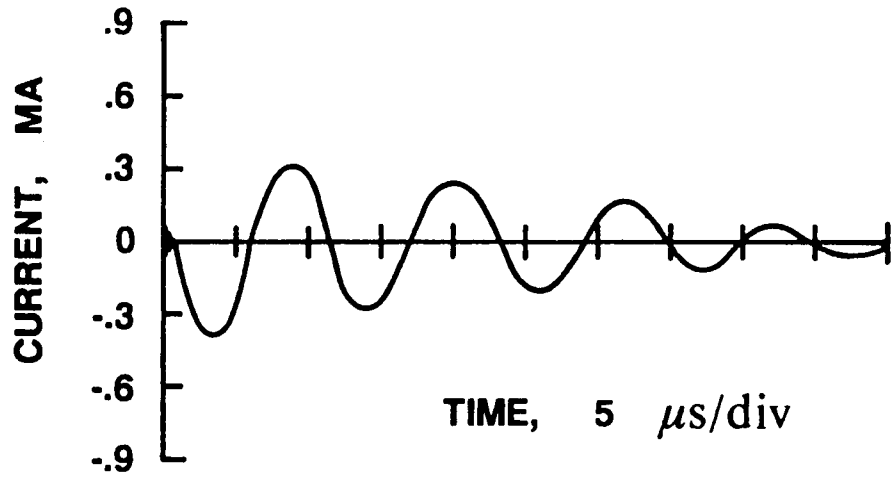

SYSTEM PARAMETERS:

PRESSURE: p = 20 mTorr

CHARGING VOLTAGE: E = 14kV

CAPACITANCE: C = 48.6 μF

RINGING FREQUENCY: f = 78 kHz

CIRCUIT INDUCTANCE: L = 85.4 nH

RISE TIME: t = 3.2 μs

PEAK CURRENT: I = 333 kA

Figure 11. Main current signal (with ring trigger)

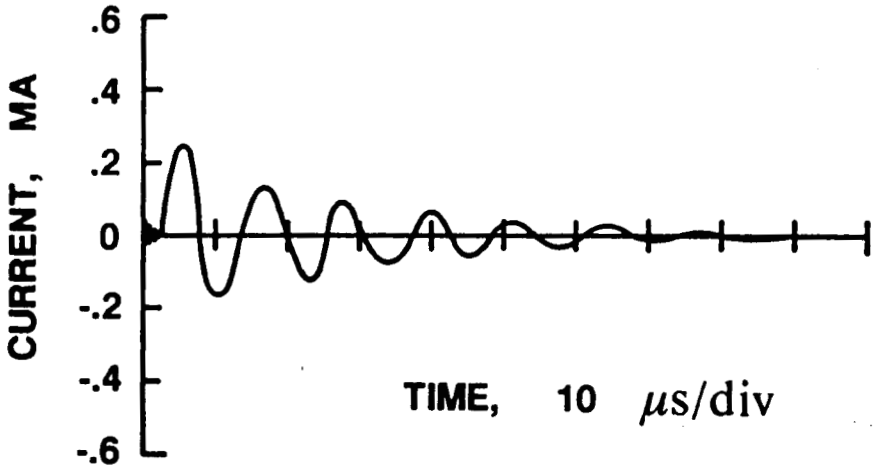

SYSTEM PARAMETERS:

PRESSURE: p = 180 Torr

CHARGING VOLTAGE: E = 9 kV

CAPACITANCE: C = 48.6 μF

RINGING FREQUENCY: f = 83 kHz

CIRCUIT INDUCTANCE: L = 75.6 nH

RISE TIME: t = 3 μs

PEAK CURRENT: I = 230 kA

Figure 12. Main current signal (with wire-brush trigger)

a good plasma source in many other applications. Subsequently, the combination of the inverse-pinch switch and HCP device as a trigger is a perfect match. Figure 13 shows a three-dimensional cut-away view of the HCP^3 which was attached to the inverse-pinch switch (Fig. 1 which shows a cross section of the overall picture).

The initial current over the HCP insulator is produced by a surface flash-over due to an applied over-voltage. The current-sheet is then compressed towards the axial column of the main switch inner electrode by the ponderomotive force ($\vec{J} \times \vec{B}$) which is created by the interaction of the induced field with the current density. This compressed plasma sheet eventually reaches the annular opening of the HCP^3 trigger which faces the gap between the inner and outer electrodes of the switch, and then is injected into the gap to connect the main electrodes of the switch.

Various sizes (from 5 cm to 15 cm diameters) of the HCP^3 trigger, which is coaxial and located below the outer electrode of the inverse-pinch switch, have been tested to find the optimal pressure range for uniform breakdown. In general, the test results show that an HCP^3 trigger with a large diameter (15 cm, which is the diameter measured at the outer end where the initial connection of trigger current takes place over the HCP insulator) has less frequent uniform breakdown than that an HCP^3 trigger with a small diameter.

A large diameter HCP^3 trigger requires a high energy input to initiate a surface flash over the HCP insulator. The energy requirement of the HCP^3 trigger is approximately proportional to the square of the diameter of the HCP insulator. For instance, consider a trigger pulse generator that can deliver 100 J of energy to the HCP^3 trigger whose insulator has an outer diameter of 15 cm and width of 2 cm. The energy density over the HCP insulator, at break down, is 2.27 J/cm^2. With the same energy input from a trigger pulse generator, the HCP^3 which has the diameter of 5 cm and a 2 cm wide circular strip insulator has an energy density of 8 J/cm^2. As in this example, the reduction of the HCP outer diameter is desirable for the use of a fixed trigger pulse. On the other hand, the long arc runner distance with a large outer diameter of an HCP^3 is desirable to obtain sufficient

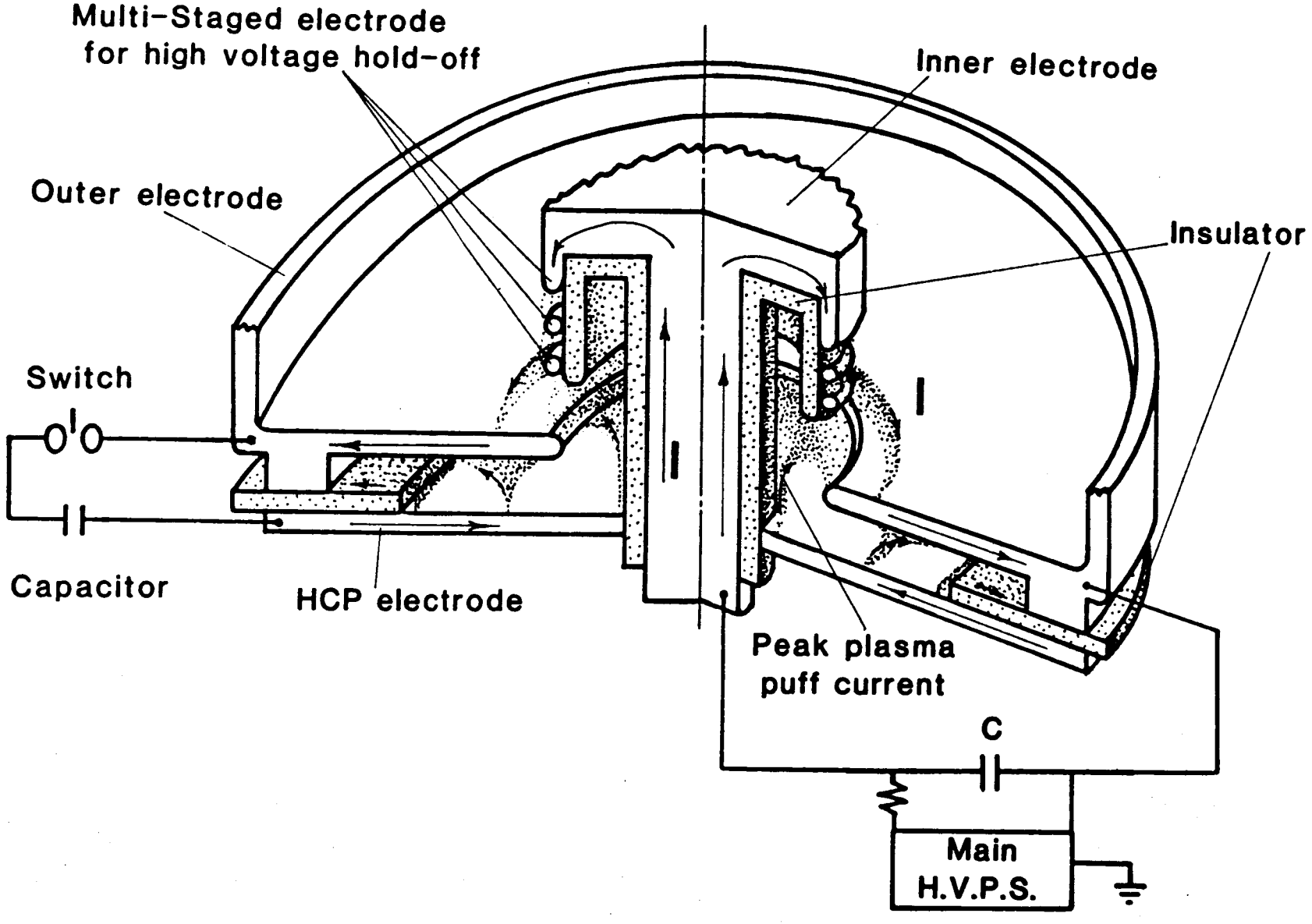

Figure 13. HCP imploding accelerator for plasma puff

formative time for the HCP plasma which is eventually injected into the gap between the main inner and outer electrodes. This formative time of the HCP plasma is necessary for a uniform, high density plasma. However, the longer the formative time, the more noise is generated and the longer the delay. The noise may be prevented by an all metal chamber of the HCP^3 trigger but some leakage of noise still appeared in the experimental data (Fig. 14). As a result, a small outer diameter HCP^3 switch is suitable for uniform breakdown with low noise and short delay. Delays to the main switching are mainly related to the chamber gas pressure and discharge voltage. The velocity of the current sheet in the HCP device is proportional to the discharging voltage and inversely proportional to the square root of the HCP pressure. Accordingly, for the same distance traveled by the current sheet to the inner annular opening of the HCP which faces the gap between the inner and outer electrodes of the switch, the time delay is proportional to the square root of the HCP pressure and inversely proportional to the discharging voltage.That is, the time delay $\triangle t_d$ is

$$\triangle t_d \propto \frac{\sqrt{p}}{E} \tag{23}$$

where p is the HCP chamber pressure and E is the discharge voltage.

Figure 15 shows the delay time of the switch at three different pressures of nitrogen gas. Figure 14 shows that higher pressure results in greater delay. The charging voltage rate on the x-axis of Fig. 14 represents the ratio of the discharge voltage to the self breakdown voltage. Accordingly, one can find the data points for 50 torr pressure which clearly show the inverse proportionality of the delay time with respect to the discharge voltage.

In this case, the size of the HCP electrode is limited only by the diameter of the main electrode column in the inverse-pinch switch. Figure 16 shows the ICC frame mode pictures for non-uniform breakdown of the HCP^3 having a diameter of 15 cm, at various pressures. These pictures reveal that the trigger pulse energy from the mini-Marx generator was not

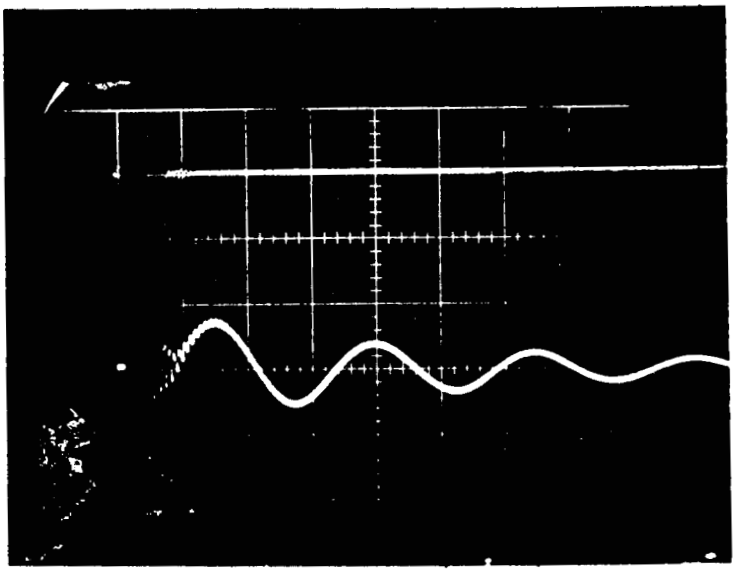

Figure 14. Switch current reading (200 torr 6.5 kV, main, 4.5 kV trigger, 5 V/div.) leading edge of wave form shows noise carrier

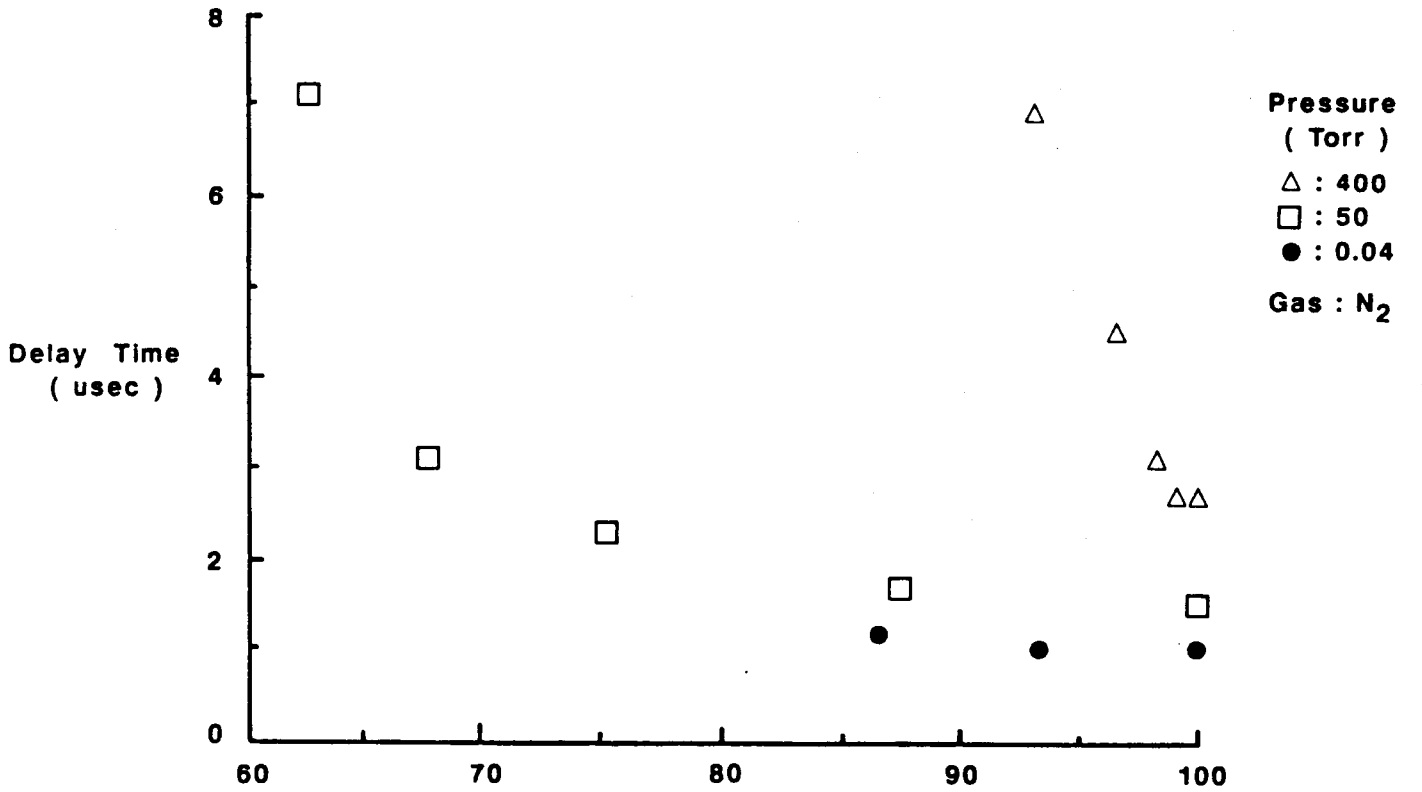

Figure 15. Delay time with respect to discharging voltage vs. self breakdown voltage at various pressures

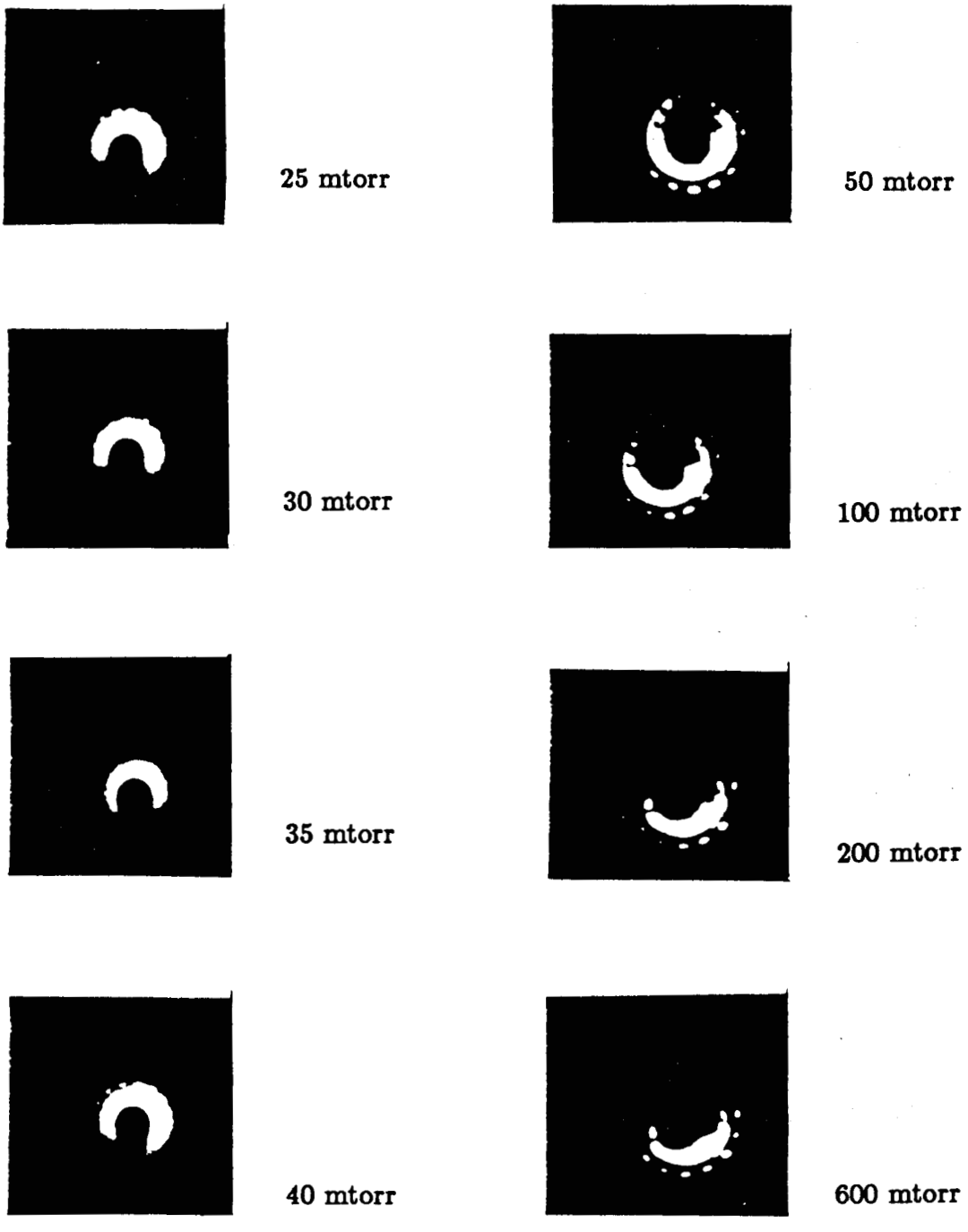

Figure 16. Triggering discharge profiles at different pressures using focus mode of image converter camera (exposure time 200 nsec trigger voltage 148 kV)

sufficient for the size of the HCP[3] trigger to form a uniform initiation of breakdown.

IV. CONCLUSIONS AND RECOMMENDATIONS

The computer simulation code for the theoretical analysis of an inverse-pinch plasma switch was developed using a 2-dimensional, two-temperature MHD model. The application of the code was made for the disk-type inverse-pinch switch geometry. The results from the computer simulation of the disk-type switch are generally in agreement with the measured data in the experiment. Further applications of the code to the other inverse-pinch geometries and the generalization of the code in use are recommended.

An inverse-pinch plasma switch for closing has been designed and tested for high-power switching requirements. Successful development of the inverse-pinch plasma switch mainly depends on a trigger which produces an azimuthally uniform initiation of breakdown for an inverse-pinch current path in the switch.

The types of triggers which were tested are trigger pins, wire-brush trigger, ring trigger, and hypocycloidal-pinch (HCP) plasma puff trigger. Among the triggers tested, the HCP plasma puff was the only one which successfully produced an azimuthally uniform plasma-ring (or ring-shaped plasma puff) and injected the plasma-ring into the gap of the switch electrodes for a uniform breakdown.

The diameter of the HCP devices as a trigger is a factor that also determines uniform breakdown. Various sizes (from 5-cm to 15-cm diameter) of the HCP^3 trigger, which is coaxially located below the outer electrode of the inverse-pinch switch, have been tested to find the optimal pressure range for uniform breakdown. The results indicate that the HCP^3 with a large diameter has less frequent uniform breakdown than that of an HCP^3 trigger with a small diameter.

Further study of the HCP^3 trigger is still necessary to determine the size, the range of fill gas pressure, the delay time, the noise, and the gap distance for uniform breakdown. These are indeed crucial for the inverse-pinch current path in the switch.

REFERENCES

1. Choi, S. H. and J. H. Lee, "An Inverse-Pinch Switch for High Coulomb Transfer," *Proc. of the 10th IEEE International Symposium on Discharges and Electrical Insulation in Vacuum*, Columbia, SC, p. 273, Oct. 25-28, 1982.
2. Lee, J. H. and S. H. Choi, "A Surface-Discharge Triggered Inverse-Pinch Switch," *The 26th Annual Meeting of the Division of Plasma Physics of the American Physical Society (APS/OPP)*, Boston, MA, Oct. 29-Nov. 2, 1984.
3. Schuster, G. L., J. H. Lee and S. H. Choi, "Inverse-Pinch Plasma Switch," *Proc. of the 5th IEEE Pulsed Power Conf.*, June 10-12, 1985.
4. Braginskii, S. I., "Transport Phenomena in a Completely Ionized Two-Temperature," *Soviet Physics JETP*, Vol. 6 (33), No. 2, Feb. 1958.
5. Spitzer, L., *Physics of Fully Ionized Gases*, Interscience, NY, p. 143, 1962.
6. Maxon, S., "Bremsstrahlung Rate and Spectra From a Hot Gas ($Z = 1$)," *Physical Review A*, Vol. 5, No. 4, Apr. 1978.
7. Choi, S. H. and J. H. Lee, "A Long Life Plasma Switch for Space Applications," *22nd IECEC Proceedings*, Vol. 1, Aug. 10-14, 1987.
8. Lee, J. H., "Hypocycloidal-Pinch Device," U. S. Patent No. 4,042,848, issued Aug. 16, 1977.
9. Lee, J. H., D. R. McFarland and R. J. DeYoung, "Atomic Flow Line Laser Pumped by a Hypocycloidal-Pinch Array," *J. Opt. Soc. Am.*, 70, 1621, 1980.
10. Lee, J. H., "A High Coulomb Transfer Switch," U. S. Patent No. 4,475,066, issued Oct. 2, 1984.

NASA National Aeronautics and Space Administration

Report Documentation Page

1. Report No.	2. Government Accession No.	3. Recipient's Catalog No.
NASA CR-181768		

4. Title and Subtitle	5. Report Date
Development and Simulation Study of a New Inverse-Pinch High Coulomb Transfer Switch	May 1989
	6. Performing Organization Code

7. Author(s)	8. Performing Organization Report No.
Sang H. Choi	FR 688102
	10. Work Unit No. 506-41-41-02

9. Performing Organization Name and Address	11. Contract or Grant No.
Information & Control Systems, Incorporated 28 Research Drive Hampton, VA 23666	NAS1-17685
	13. Type of Report and Period Covered
12. Sponsoring Agency Name and Address	Contractor Report
National Aeronautics and Space Administration Langley Research Center Hampton, VA 23665-5225	14. Sponsoring Agency Code

15. Supplementary Notes

Langley Technical Monitor: W. E. Meador
Final Report

16. Abstract

A theoretical study of the inverse-pinch plasma switch was conducted using a computer simulation code. The code was based on a 2-D, 2-temperature magnetohydrodynamic (MHD) model. The application of this code was limited to the disk-type inverse-pinch plasma switch. The results of the computer analysis appear to be in agreement with the experimental results when the same parameters are used.

A novel inverse-pinch plasma switch for closing has been designed and tested for high-power switching requirements. An azimuthally uniform initiation of breakdown is a key factor in achieving an inverse-pinch current path in the switch. Thus, various types of triggers, such as trigger pins, wire-brush, ring trigger, and hypocycloidal-pinch (HCP) devices have been tested for uniform breakdown.

Recently, triggering was achieved by injection of a plasma-ring (plasma puff) that is produced separately with hypocycloidal-pinch electrodes placed under the cathode of the main gap. The current paths at switch closing, initiated by the injection of a plasma-ring from the HCP trigger are azimuthally uniform, and the local current density is significantly reduced, so that damage to the electrodes and the insulator surfaces is minimized. The test results indicate that electron bombardment on the electrodes is four orders of magnitude less than that of a spark-gap switch for the same switching power. Indeed, a few thousand shots with peak current exceeding a mega-ampere and with hold-off voltage up to 20 kV have been conducted without showing measurable damage to the electrodes and insulators.

17. Key Words (Suggested by Author(s))	18. Distribution Statement
Inverse-pinch plasma switch Hypocycloidal-pinch (HCP) trigger Inverse-pinch spark-gap	Unclassified – Unlimited Subject Category 75

19. Security Classif. (of this report)	20. Security Classif. (of this page)	21. No. of pages	22. Price
Unclassified	unclassified	45	A03

Report Documentation Page

NASA National Aeronautics and Space Administration

1. Report No.	2. Government Accession No.	3. Recipient's Catalog No.
NASA CR-181768		

4. Title and Subtitle	5. Report Date
Development and Simulation Study of a New Inverse-Pinch High Coulomb Transfer Switch	May 1989
	6. Performing Organization Code

7. Author(s)	8. Performing Organization Report No.
Sang H. Choi	FR 688102
	10. Work Unit No. 506-41-41-02

9. Performing Organization Name and Address	11. Contract or Grant No.
Information & Control Systems, Incorporated 28 Research Drive Hampton, VA 23666	NAS1-17685
	13. Type of Report and Period Covered
12. Sponsoring Agency Name and Address	Contractor Report
National Aeronautics and Space Administration Langley Research Center Hampton, VA 23665-5225	14. Sponsoring Agency Code

15. Supplementary Notes

Langley Technical Monitor: W. E. Meador
Final Report

16. Abstract

~~A theoretical study of~~ the inverse-pinch plasma switch was ~~conducted~~ studied using a computer simulation code. The code was based on a 2-D, 2-temperature magnetohydrodynamic (MHD) model. The application of this code was limited to the disk-type inverse-pinch plasma switch. The results of the computer analysis appear to be in agreement with the experimental results when the same parameters are used.

~~A novel~~ inverse-pinch plasma switch for closing has been designed and tested for high-power switching requirements. An azimuthally uniform initiation of breakdown is a key factor in achieving an inverse-pinch current path in the switch. Thus, various types of triggers, such as trigger pins, wire-brush, ring trigger, and hypocycloidal-pinch (HCP) devices have been tested for uniform breakdown.

Recently, triggering was achieved by injection of a plasma-ring (plasma puff) that is produced separately with hypocycloidal-pinch electrodes placed under the cathode of the main gap. The current paths at switch closing, initiated by the injection of a plasma-ring from the HCP trigger are azimuthally uniform, and the local current density is significantly reduced, so that damage to the electrodes and the insulator surfaces is minimized. The test results indicate that electron bombardment on the electrodes is four orders of magnitude less than that of a spark-gap switch for the same switching power. Indeed, a few thousand shots with peak current exceeding a mega-ampere and with hold-off voltage up to 20 kV have been conducted without showing measurable damage to the electrodes and insulators.

17. Key Words (Suggested by Author(s))	18. Distribution Statement
Inverse-pinch plasma switch Hypocycloidal-pinch (HCP) trigger Inverse-pinch spark-gap	Unclassified – Unlimited Subject Category 75

19. Security Classif. (of this report)	20. Security Classif. (of this page)	21. No. of pages	22. Price
Unclassified	unclassified	45	A03

NASA FORM 1626 OCT 86